ELSEVIER

Journal of Power Sources 66 (1997) 159–164

JOURNAL OF POWER SOURCES

Short Communication

Influence of bismuth on hydrogen and oxygen evolution on lead–calcium–tin–aluminium grid alloys

S. Zhong [a], J. Wang [a], H.K. Liu [a], S.X. Dou [a], M. Skyllas-Kazacos [b]

[a] *Institute for Materials Technology and Manufacturing, University of Wollongong, Wollongong, NSW 2522, Australia*

[b] *School of Chemical Engineering and Industrial Chemistry, University of New South Wales, Sydney, NSW 2052, Australia*

Received 15 August 1996; accepted 20 September 1996

Abstract

Hydrogen and oxygen evolution on lead–calcium–tin–aluminium alloys with different bismuth additions, in the range 0.002 to 0.073 wt.%, in sulfuric acid solutions at room temperature have been investigated. Hydrogen evolution rates are measured by linear sweep voltammetry. Kinetic parameters of the hydrogen evolution reaction on electrodes show that the incorporation of bismuth in the alloys decreases the hydrogen overpotential and increases the hydrogen evolution rate. Oxygen evolution rates are measured by a step-potentiostatic method, together with gas collection. The results show that oxygen evolution rates are enhanced by the bismuth additions and also influenced by the quantity of lead dioxide on the electrode surface. The effect of structure of the alloy surface on hydrogen evolution rate is also discussed.

Keywords: Hydrogen evolution; Oxygen evolution; Bismuth; Grid alloy; Lead; Calcium; Tin; Aluminium

1. Introduction

Hydrogen and oxygen evolution in lead/acid batteries take place as side reactions during battery charge, and produce water loss. The gassing properties of grid alloys are of particular concern in valve-regulated lead/acid batteries (VRLAs). Most minor elements in lead alloys, whether impurities from lead or alloy additives, decrease the hydrogen overpotential and enhance hydrogen evolution. If such unwanted properties are negligible or tolerable, however, these elements can be accepted and employed effectively in grid alloys for other beneficial effects that they provided, such as improvement in the mechanical properties, the corrosion properties, and battery performance. Initially, bismuth was considered as a detrimental element in lead/acid batteries. Because of its chemical similarity to lead, the removal of bismuth from lead to a level of below 250 ppm is both difficult and expensive [1]. More recent studies have, however, suggested that bismuth may have beneficial effects on battery performance. A better understanding of its effect on the gassing properties of lead/acid batteries is still needed.

Kilimnet and Rominyan [2] found that the kinetic constants of the hydrogen evolution reaction (a and b in the Tafel equation, $\eta = a + b \times \log i$), depend on the magnitude of charge on the electrode surface, and the constants indicate a low rate of hydrogen gas formation. Rice [1] reported that bismuth reduced the oxygen evolution overpotential but increased hydrogen evolution overpotential on lead–bismuth alloys. The critical level for the former was 0.6 wt.% Bi and 0.06 wt.% Bi for the latter. Papageorgiou and Skyllas-Kazacos [3] investigated the effects of bismuth on the hydrogen evolution reaction rates and correlated the effects with electrode surface morphology and macrostructure. The results concluded that bismuth additions decreased the hydrogen overpotential on lead–bismuth alloys. Caldwell et al. [4] reported that a low bismuth content, 0.018 wt.% in refined secondary lead, had little influence on the gassing rate in lead–calcium–tin alloy battery system. Manders et al. [5] reported that by doping the active material with bismuth oxide powder in both positive and negative plates, the build-up in gas pressure was reduced in VRLAs during constant-current charging. Lam et al. [6] examined the gassing characteristics of some minor elements, including bismuth, on pure lead, lead alloys and pasted electrodes. Data provided by these authors show that the hydrogen evolution rate of the lead–bismuth binary alloy is lower than that of common lead–calcium–tin alloys and the situation in oxygen gassing rates is different. They pointed out that the manufacturing conditions of the lead alloy can exert a marked effect on the rate of hydrogen and oxygen evolution.

Bismuth effects on gassing properties have been extensively studied, but most of these investigations have been performed on lead–bismuth binary alloys [7]. The aim of the

PII S0378-7753(96)02478-0

present study is to investigate the effect of bismuth additions on hydrogen and oxygen evolution on a common lead–calcium–tin–aluminium grid alloy.

2. Experimental

Alloys and working electrodes were prepared as described previously [8]. Sample alloy rods were gravity-cast in a steel mould and cooled at room temperature. One group of alloy rods was annealed at 240 °C for 20 h and then cooled to room temperature. The other group of alloy rods were used without thermal treatment. All the alloy rods were stored at room temperature for over one month before electrode fabrication. A thick, insulated, copper wire was welded to one end of the alloy rod to make good electrical contact and hold the electrode rigidly. The specimen was then mounted in epoxy resin (Araldite) in a plastic holder with the end polished to expose the working electrode surface. The alloy compositions were analysed by inductively coupled plasma spectroscopy (ICP); the results are listed in Table 1.

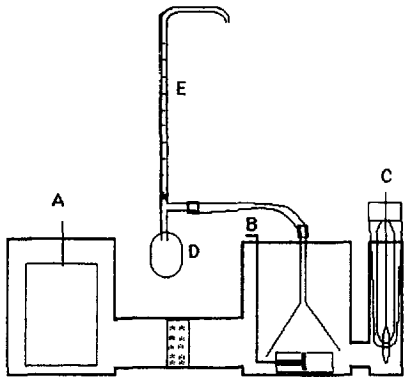

Fig. 1. Electrochemical cell used for gassing measurements: (A) counter electrode; (B) working electrode; (C) reference electrode; (D) rubber container, and (E) glass tube.

Table 1
Alloy composition by ICP analysis (wt.%)

Electrode no.	Ca	Sn	Al	Bi
1 [a]	0.071	0.383	0.016	0.002
2	0.068	0.379	0.013	0.045
3	0.064	0.374	0.010	0.059
4	0.064	0.362	0.016	0.073

[a] A normal grid alloy: all samples were prepared from this alloy.

The method of surface treatment described previously [8] was employed throughout the experiments. A three-compartment cell, separated by glass frits, was used. The reference electrode was a Hg/Hg_2SO_4 (K_2SO_4 saturated solution) electrode and all potentials refer to this electrode. The counter electrode was a sheet of pure lead. The electrolyte was 1.28 sp. gr. H_2SO_4 solution, prepared from 98 wt.% H_2SO_4 (Univar AR) with double-distilled water. The electrolyte was deaerated with high-purity nitrogen for 40 min before immersion of the test electrode in the solution.

Linear sweep voltammograms and step-potentiostatic measurements were performed by a scanning potentiostat (Model 362, EG&G Princeton Applied Research) that was connected via a MachLab/8 interface (Analog Digital Instruments, AD Instruments Pty Ltd.) to a Macintosh computer supported by Chart v3.3 software.

Hydrogen evolution rate measurements were performed after each working electrode was held initially at a potential of -1.3 V for 30 min. This treatment is used to reduce any surface oxide on the working electrode. The working electrode potential was then scanned from -1.3 to -1.8 V at a rate of 0.1 mV s^{-1}. The hydrogen evolution rate is represented by the current recorded. Since the oxygen evolution on the electrode surface is affected by the quantity of lead dioxide on the electrode surface, oxygen evolution measurements were approached in the following way: a step-potentiostatic procedure with gas collection was used, which was

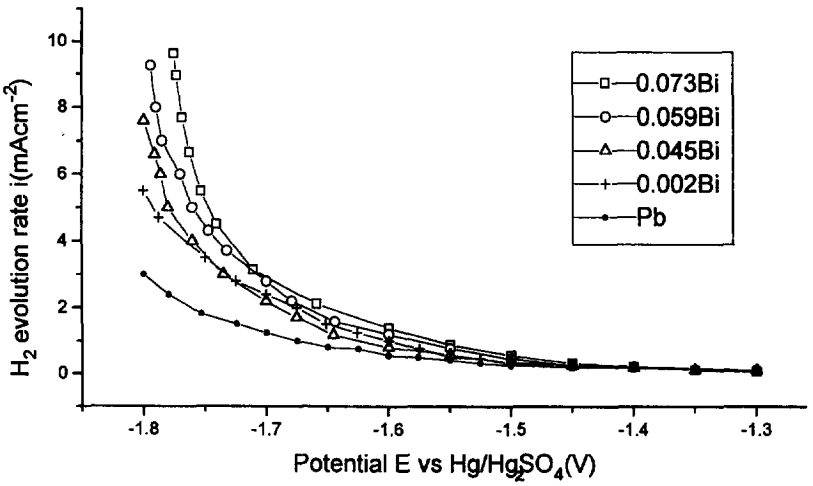

Fig. 2. Hydrogen evolution rate on pure lead and different bismuth alloy electrodes (untreated); sweep rate = 0.1 mV s^{-1} in 1.28 sp. gr. H_2SO_4.

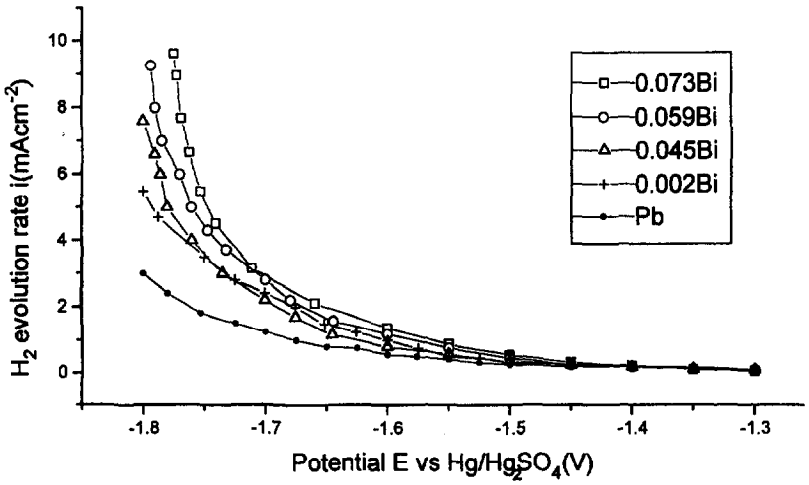

Fig. 3. Hydrogen evolution rate on pure lead and different bismuth alloy electrodes (untreated); sweep rate = 0.1^{-1} mV s^{-1} in 1.28 sp. gr. H_2SO_4.

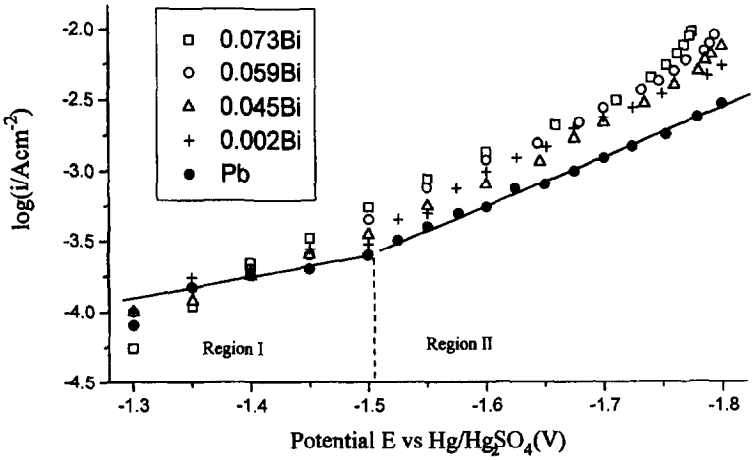

Fig. 4. Tafel plots for hydrogen evolution on untreated electrodes.

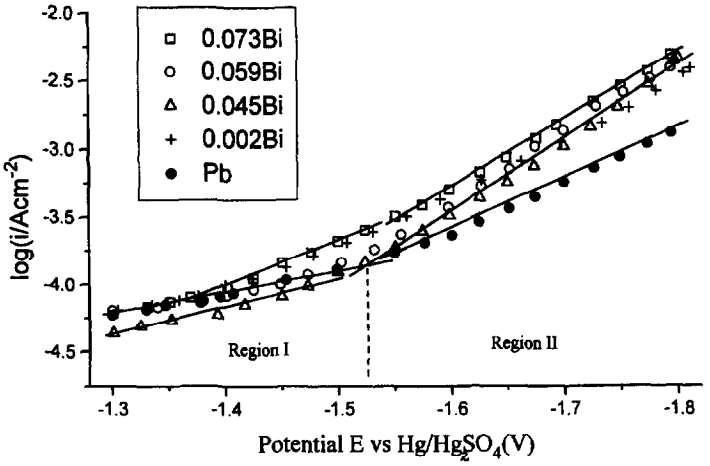

Fig. 5. Tafel plots for hydrogen evolution on thermally treated electrodes.

similar to that described by Lam et al. [6]. The difference between the two methods was that a 'soap-bubble' method was used in the gassing measurements in our experiments. This is considered to be more convenient and more accurate. A diagram of the cell for the gassing measurement is shown in Fig. 1.

The oxygen evolution current density, i_{O_2}, according to Faraday's law, is calculated by

$$i_{O_2}(\mathrm{A\ cm^{-2}}) = [4F\,(P_{atm} - P_w)V]/(RTAt) \quad (1)$$

where P_{atm} is the atmospheric pressure; P_w is the vapour pressure at the absolute temperature T; F is the Faraday constant; V is the gas volume measured by the 'soap-bubble method' in m^3; R is the gas constant (= 8.314 J mol^{-1} K^{-1}); t is the electrolysis time (in s); A is the electrode area (in cm^2).

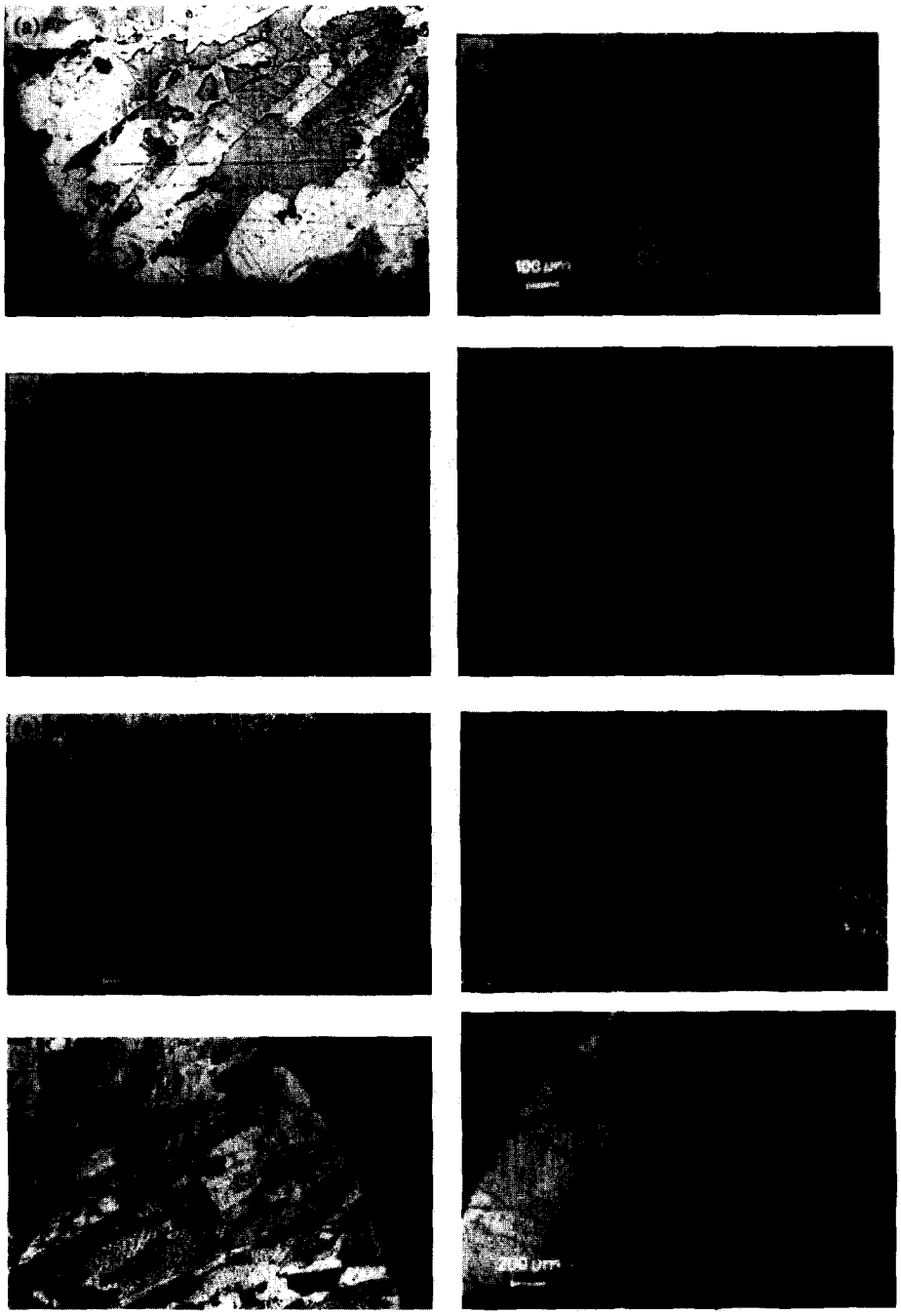

Fig. 6. Metallurgical structure of alloy electrodes: (a) non-thermally treated alloy 0.002 wt.% Bi; (b) thermally treated alloy Bi = 0.002 wt.% Bi; (c) non-thermally treated alloy 0.059 wt.% Bi; (d) thermally teated alloy 0.059 wt.% Bi; (e) non-thermally treated alloy 0.073 wt.% Bi; (f) thermally treated alloy 0.073 wt.% Bi; (g) non-thermally treated 0.045 wt% Bi, and (h) non-thermally treated pure lead.

3. Results and discussion

3.1. Hydrogen evolution reaction rate

The rate of the hydrogen evolution reaction on the untreated electrodes and on the thermally-treated electrodes is presented in Figs. 2 and 3, respectively. The corresponding Tafel plots are shown in Figs. 4 and 5. The Tafel slope, b, and the exchange-current density, i_0, which represent the kinetics of the hydrogen evolution reaction are listed in Tables 2 and 3. These results show that the hydrogen evolution rates are enhanced by the bismuth additions for both untreated and thermally-treated electrodes. Compared with untreated electrodes the thermal treatment process causes an increase in the hydrogen evolution overpotential and, therefore, decreases the hydrogen evolution rate. The Tafel plots exhibit two distinct linear region, one at lower potentials, the other at higher potentials. This behaviour is consistent with results observed by Papageorgiou and Skyllas-Kazacos [3] and Lam et al. [6].

The metallurgical microstructure of the electrodes, both thermally treated and untreated, are shown in Fig. 6. A slight

Table 2
Tafel parameter values for hydrogen evolution reaction on untreated electrodes

Electrode no.	Region I		Region II	
	b (V)	$\log(i_0, A\,cm^{-2})$	b (V)	$\log(i_0, A\,cm^{-2})$
1	−0.390	−5.12	−0.234	−5.92
2	−0.309	−5.03	−0.194	−6.56
3	−0.405	−4.81	−0.222	−6.19
4	−0.499	−4.79	−0.189	−5.67
Pb	−0.547	−5.76	−0.249	−6.76

Table 3
Tafel parameter values for hydrogen evolution reaction on thermally treated electrodes

Electrode no.	Region I		Region II	
	b (V)	$\log(i_0, A\,cm^{-2})$	b (V)	$\log(i_0, A\,cm^{-2})$
1	−0.685	−5.25	−0.231	−6.36
2	−0.572	−5.17	−0.194	−7.04
3	−0.679	−5.12	−0.182	−7.01
4	−0.487	−5.06	−0.216	−6.39
Pb	−0.489	−5.93	−0.283	−7.22

increase in grain size can been seen in the thermally treated alloy. The grain boundaries of the thermally treated samples are more regular and the columnar crystals with clear crystal orientation due to the casting are observed. The enhancement effect on the hydrogen evolution overpotential of the thermally treated alloys is therefore attributed to the variations in the alloy surface structure due to the annealing process. This indicates that 'the effective active area' for hydrogen evolution on the electrode surface could be reduced by the thermal treatment process, i.e., both casting and cooling (or thermal treatment) conditions can affect the degree of segregation of the constituent elements in the grain boundaries of the alloys and this, in turn, influences the rate of hydrogen evolution, as described by Lam et al. [6].

3.2. Oxygen evolution reaction rates

The results of the oxygen evolution rate measurements from the gas-collection experiments are presented in Fig. 7. The results from the oxygen evolution measurements show that the bismuth additions also enhance oxygen evolution and the enhancement is proportional to the bismuth additions. As described by Manders et al. [5], the bismuth additions could improve the gas recombination in VRLAs. The oxygen evolution efficiency, σ, during charging is calculated by the ratio, $\sigma = Q_{O_2}/Q_t$, where Q_{O_2}, is the coulombs calculated from the gas volume collected according to the Tafel equation and Q_t is the total number of coulombs recorded during the charging.

Table 4
Oxygen evolution efficiency (%) at different potentials

Electrode potential (V)	Electrode no.			
	1	2	3	4
1.55	80.5	91.9	87.8	86.9
1.60	86.7	92.2	88.3	87.4
1.65	88.9	93.8	89.5	94.1
1.70	90.2	95.3	89.4	91.8
1.75	92.5	95.4	90.8	94.9
1.80	97.3	95.6	94.6	96.8

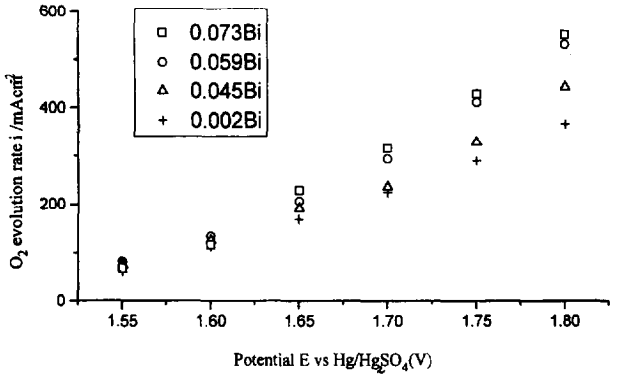

Fig. 7. Oxygen evolution rate on electrodes with different bismuth contents.

The data are listed in Table 4. The results show that the current efficiency for oxygen evolution is lower at the lower potentials since the lead electrode reactions are consuming some of the current. At higher potential, however, oxygen evolution becomes more dominant, so the current efficiency increases.

4. Conclusions

1. Hydrogen evolution on a common lead–calcium–tin–aluminium alloy, both thermally treated and untreated, is enhanced by bismuth additions.
2. The thermal treatment process used in the experiments affected the degree of segregation of the elements in the grain boundaries of the alloys, slightly modified the microstructure of the alloys, and decreased the hydrogen evolution rates.
3. Oxygen evolution is enhanced by the bismuth additions.
4. The oxygen evolution rates are also dependent on the quantity of lead dioxide on the electrode surface and the oxygen evolution efficiency is higher at higher overpotentials and lower at lower overpotentials.

References

[1] D.M. Rice, *J. Power Sources, 28* (1989) 69.
[2] A.B. Kilimnik and A.L. Rominyan, *Elektrokhimiya, 5* (1969) 1234.

[3] N. Papageorgiou and M. Skyllas-Kazacos, *Electrochim. Acta., 37* (1992) 269.
[4] T.W. Caldwell, U.S. Sokolov and L.M. Bocciarelli, *J. Electrochem. Soc., 123* (1976) 1265.
[5] J.E. Manders, L.T. Lam, R. De Marco, J.D. Douglas, R. Pillig and D.A.J. Rand, *J. Power Sources, 48* (1994) 113.
[6] L.T. Lam, R. De Marco, J.D. Douglas, R. Pillig and D.A.J. Rand, *J. Power Sources, 48* (1994) 219.
[7] M.J. Koop, D.A.J. Rand and B. Culpin, *J. Power Sources, 45* (1993) 365.
[8] S. Zhong, H.K. Liu, S.X. Dou and M. Skyllas-Kazacos, *J. Power Sources, 59* (1996) 123.